Available online at www.sciencedirect.com
SCIENCE DIRECT®
Journal of Sound and Vibration 267 (2003) 961–966
JOURNAL OF SOUND AND VIBRATION
www.elsevier.com/locate/jsvi

Letter to the Editor

Shear effects in aeroacoustic predictions

B.A. Singer*, D.P. Lockard

Computational Modeling and Simulation Branch, NASA Langley Research Center, MS 128, Hampton, VA 23681-2199, USA

Received 10 January 2003; accepted 16 January 2003

1. Introduction

An increasingly popular trend has been to employ hybrid methods for aeroacoustic predictions. A hybrid acoustic prediction combines the use of unsteady computational fluid dynamics for calculating the properties of acoustic sources with some form of Lighthill's acoustic analogy [1] to calculate the resulting farfield noise radiation from an integration of the nearfield solution. In principle, the unsteady fluid dynamic calculation properly resolves all aerodynamic noise sources, including acoustic/mean-flow interactions. In practice, the computing resources required to properly resolve sound waves all the way to the free stream, where the flow is uniform, is often prohibitive. As a consequence, the acoustic analogy is often applied in a manner that is not strictly correct; i.e., all of the acoustic sources are not included. In particular, the effects of regions with minimal hydrodynamic unsteadiness, but with significant mean-flow gradients are often neglected (see Ref. [2,3]). Here we discuss a simple two-dimensional flow where the effects of neglected shear can be quantified. Extensions of this simple flow can be used to develop guidelines as to what levels of errors might be incurred in practical applications.

2. The flow and acoustic solvers

A spatially seven-point, sixth-order accurate finite difference code was used to solve the frequency-domain version of the Euler equations linearized about an imposed mean flow. The code uses Runge–Kutta time stepping to march to a steady state, and employs many of the acceleration techniques employed in computational fluid dynamics (CFD) calculations. The code is similar to that developed by Agarwal and Huh [4]. Analytic solutions for cases with no mean flow agreed with the finite difference results to better than 1% over the entire domain of interest for the grid used in this test. Comparisons with a second order accurate finite difference code for one test case that included the mean flow showed differences of approximately 10 percent of the peak, but all the qualitative features of the flow were replicated by the two codes.

*Corresponding author.

0022-460X/03/$ - see front matter
doi:10.1016/S0022-460X(03)00216-5

The farfield noise was computed by solving the Ffowcs Williams and Hawkings [5] (hereafter referred to as FW–H) equation. The FW–H equation is one of the most general forms of Lighthill's acoustic analogy. From a computational perspective, solving the FW–H equation is attractive because, with a small amount of approximation, the volumetric integration required to solve Lighthill's original equation [6] is reduced to a surface integration. In the hybrid technique, surface data provide the link between the unsteady CFD code and the acoustic field solver.

Following Brentner and Farassat [7], the FW–H equation may be written in differential form as

$$\Box^2 p'(\mathrm{x},t) = \frac{\partial^2}{\partial x_i \partial x_j}[T_{ij}H(f)] - \frac{\partial}{\partial x_i}[L_i\delta(f)] + \frac{\partial}{\partial t}[(\rho_0 U_n)\delta(f)], \tag{1}$$

where $\Box^2 \equiv \frac{1}{c^2}\frac{\partial^2}{\partial t^2} - \nabla^2$ is the wave operator, c is the ambient speed of sound, t is observer time, p' is the acoustic pressure, ρ' is the perturbation density, ρ_0 is the free-stream density, $f = 0$ defines an arbitrary permeable data surface, $\delta(f)$ is the Dirac delta function, and $H(f)$ is the Heaviside function. The quantities U_i and L_i are defined as

$$U_i = \left(1 - \frac{\rho}{\rho_0}\right)v_i + \frac{\rho u_i}{\rho_0} \tag{2}$$

and

$$L_i = P_{ij}\hat{n}_j + \rho u_i(u_n - v_n) \tag{3}$$

respectively. In the above equations, ρ is the total density, ρu_i is the momentum in the i direction, v_i is the velocity of the data surface $f = 0$, and P_{ij} is the compressive stress tensor. For an inviscid fluid, $P_{ij} = p'\delta_{ij}$ where δ_{ij} is the Kronecker delta. The subscript n indicates the projection of a vector quantity in the surface-normal direction. To solve Eq. (1), the first term on the right-hand side should be integrated over the volume outside the data surface $f = 0$ wherever the Lighthill stress tensor T_{ij} is non-zero in this region. Alternatively, the data surface $f = 0$ can be expanded to include all regions of non-zero T_{ij}. The main objective of this work is to explore what levels of errors are incurred if the T_{ij} term is neglected and the data surface $f = 0$ does not include shear layers in the flow, where $T_{ij} \neq 0$. Hence, in this work, only the last two terms on the right-hand side of Eq. (1) are integrated. Because these two right-hand side terms are only evaluated on the data surface, the data surface serves as the means by which information is transferred from the unsteady flow calculation to the FW–H solver.

To reduce the computational effort required, the test case considered involves a two-dimensional flow. Therefore, the two-dimensional frequency-domain FW–H solver of Lockard [8] was used to compute the farfield noise distribution. This FW–H solver has been verified with a number of test cases described in Ref. [8].

3. The shear-flow test problem

An overview of the test problem is shown in Fig. 1. A two-dimensional, single-frequency acoustic source has a Gaussian amplitude distribution centered at the origin. The non-

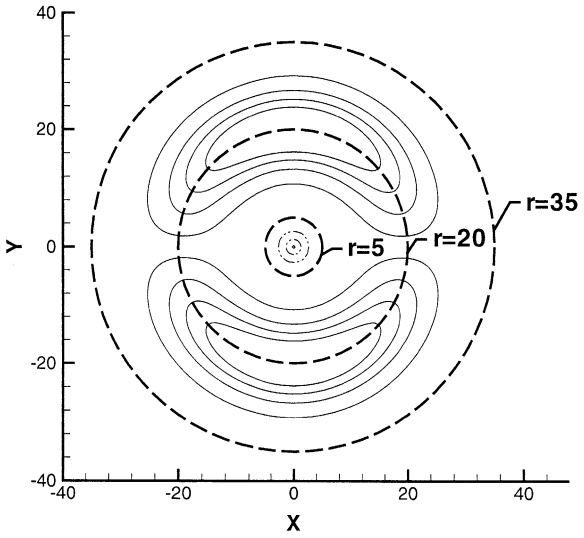

Fig. 1. Overview of test problem; — · · — · · —, contours of acoustic source function; ——, contours of azimuthal velocity of mean flow; - - - - -, data surfaces used in FW–H computation.

dimensional frequency and wavelength of the acoustic source are both unity. Intensity contours of the source are shown with dash-dotted lines in the figure. An imposed mean flow of azimuthal velocity u_θ (u_θ contours shown with solid lines) has a Gaussian distribution in the radial direction and a sinusoidal variation in the azimuthal direction, such that

$$u_\theta = U_0 \exp[-\ln(2)/b^2(r - r_t)^2] \sin\theta, \tag{4}$$

where U_0 is the maximum azimuthal speed, b is the radial distance in which u_θ drops to half of U_0, r is the distance from the origin, r_t is the radial distance of maximum u_θ, and θ is the azimuthal angle measured counterclockwise from the positive x axis. All velocities are normalized with the ambient speed of sound, and all distances with the acoustic wavelength in the ambient medium. The distribution shown in the figure was produced with $b = 5$ and $r_t = 20$. A corresponding mean density distribution was also imposed through the use of isentropic flow relations.

The velocity distribution in Eq. (4) was chosen to be at least mildly representative of flow over a body. In the coordinates of Fig. 1, the dominant flow direction is from right to left and is symmetric about $y = 0$.

The solution of the Euler-solver was sampled on three data surfaces, indicated in Fig. 1 by dashed lines. Each data surface included 721 points. Results obtained using 361 points on each data surface were plottably indistinguishable. The innermost data surface at $r = 5$ is outside the distributed source region, but inside the mean-flow annulus. The outermost data surface at $r = 35$ is outside both the distributed source region and the mean-flow annulus. The middle data surface at $r = 20$ passes through the mean-flow annulus. The flow quantities on the data surfaces were then used as input into the two-dimensional FW–H solver of Lockard [8] to compute the farfield noise distribution.

4. Results

Illustrative results for farfield noise are shown in Fig. 2. Acoustic waves seen on the innermost data surface have not yet propagated through the shear layer, so the farfield noise predicted by the FW–H solver (indicated with the solid line) is predicted as if no shear layer exists. The data on the outermost data surface represent acoustic waves that have passed entirely through the region of sheared flow and are again in a quiescent medium. The predicted farfield noise (indicated with the dotted line) includes all noise sources and acoustic-flow interactions. Data obtained by using the middle data surface show acoustic waves that have propagated through some but not all of the shear layer. As expected, the shear layer biases the propagated noise so that it is louder in the general direction of the flow (to negative x). For the $r = 20$ data surface, the predicted farfield noise increases in the cross-stream directions ($\pm y$ at $x = 0$), but that increase is not observed for the $r = 35$ data surface. Tests were also conducted with data surfaces that cut the shear layer non-uniformly. For instance, Fig. 3 compares results obtained using the data surface at $r = 20$ and results obtained using a square data surface with sides $x = \pm 20.15$ and $y = \pm 20.15$. Results obtained using the square data surface are more irregular, probably resulting from the data surface cutting the shear layer non-uniformly.

Similar calculations with $b = 2$ and 1 show progressively smaller effects as the shear layer thins. Therefore, as the shear layer becomes thinner it disturbs the radiated acoustic field less. Although these results are not surprising, they represent an important step in quantifying the impact of the data surface location. At least for simple sources in subsonic flows, the effect of a shear layer is small until the shear layer thickness is several acoustic wavelengths thick.

Another interesting result is illustrated with the directivity plots shown in Fig. 4. Here, the farfield noise is computed with the outermost data surface for three different cases. The solid line

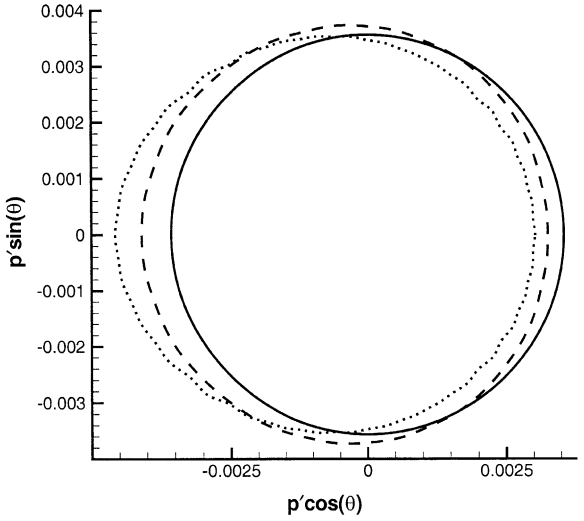

Fig. 2. Directivity plot of noise at 128 wavelengths for case of monopole-like source with shear layer defined by Eq. (4) with $U_0 = 0.5$, $b = 5.0$; ——, data surface at $r = 5$ (interior to shear layer); - - - - -, data surface at $r = 20$ (through the shear layer); ·····, data surface at $r = 35$ (outside of shear shear).

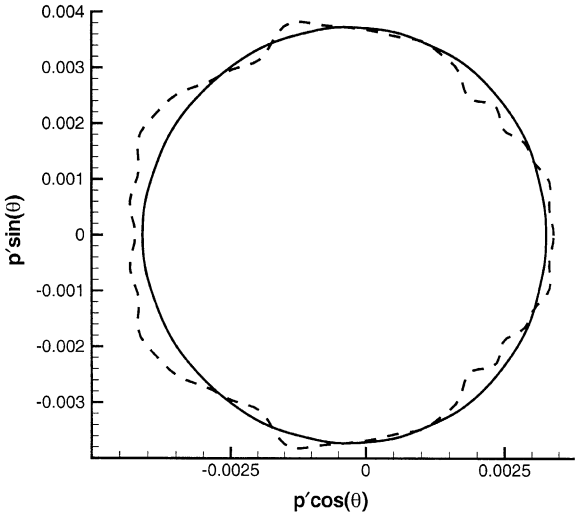

Fig. 3. Directivity plot of noise at 128 wavelengths for case of monopole-like source with shear layer defined by Eq. (4) with $U_0 = 0.5$, $b = 5.0$; ——, circular data surface at $r = 20$; - - - - -, square data surface $x = \pm 20.15$ and $y = \pm 20.15$.

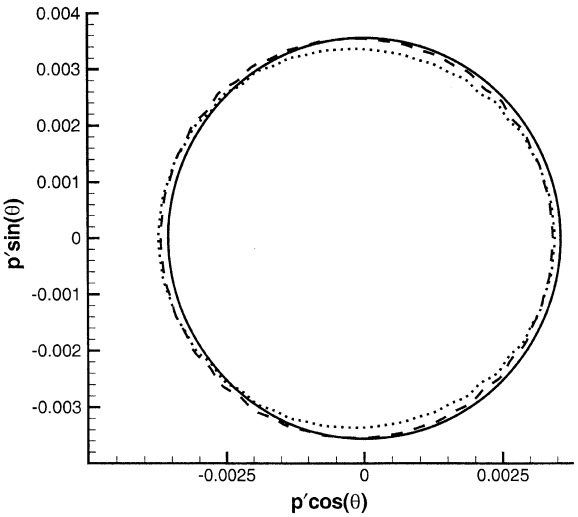

Fig. 4. Directivity plot of noise at 128 wavelengths for case of monopole-like source with shear layer defined by Eq. (4). Data surface outside of shear layer ($r = 35$); ——, $U_0 = 0$; - - - - -, $U_0 = 0.1$, $b = 5$; ·····, $U_0 = 0.5$, $b = 1$.

illustrates the case in which no shear is imposed. The dashed line shows the directivity for the case in which $U_0 = 0.1$ and $b = 5$. The dotted line illustrates the directivity for the case in which $U_0 = 0.5$ and $b = 1$. Intuitively, the effect of the shear for the dashed- and dotted-line cases might be expected to be the same. In the dashed-line case, the maximum speed in the shear layer is one-fifth that used for the case shown in Fig. 2. In the dotted-line case, the shear-layer thickness is one-fifth that used for the case shown in Fig. 2. The $\pm x$ directivities of the dashed- and dotted-line

cases coincide closely, but the $\pm y$ directivities differ noticeably; however, the $\pm y$ directivities of the no-flow case are approximately equal to those of the low-speed shear-layer case ($U_0 = 0.1$). The higher-speed shear-layer case ($U_0 = 0.5$) results in less noise being radiated in the $\pm y$ directions. Even at these relatively low speeds, the non-linear relationship of mean density to flow speed accounts for these differences. To confirm this hypothesis, another set of test cases were run. In these additional cases, the density variation in the mean flow was neglected. Under these circumstances, the directivities of the dotted- and dashed-line cases match quite closely.

5. Conclusions

A simple acoustic source distribution was surrounded by an annulus of steady shear flow. Farfield acoustics were computed by solving the Ffowcs Williams and Hawkings [5] equation using a variety of data surfaces that included varying portions of the sheared flow. Significant changes to the computed far field required the thickness of the shear layer to be several acoustic wavelengths. The directivity pattern was most distorted when the data surface cuts through the shear layer non-uniformly. If the shear-layer density is constant, decreasing the speed of the shear layer by a fixed fraction produced the same results as decreasing the thickness of the shear layer by the same fraction.

References

[1] M.J. Lighthill, On sound generated aerodynamically, I: general theory, Proceedings of the Royal Society A221 (1952) 564–587.
[2] M.R. Khorrami, M.E. Berkman, M. Choudhari, Unsteady flow computations of a slat with a blunt trailing edge, American Institute of Aeronautics and Astronautics Journal 38 (11) (2000) 2050–2058.
[3] B.A. Singer, D.P. Lockard, K.S. Brentner, Computational aeroacoustic analysis of slat trailing-edge flow, American Institute of Aeronautics and Astronautics Journal 38 (9) (2000) 1558–1564.
[4] R.K. Agarwal, K.S. Huh, Acoustic radiation due to gust-airfoil interaction in a compressible flow, CEAS/AIAA Paper-96-1755, Presented at the 2nd AIAA/CEAS Aeroacoustics Conference, State College, PA, May 6–8, 1996.
[5] J.E. Ffowcs Williams, D.L. Hawkings, Sound generated by turbulence and surfaces in arbitrary motion, Philosophical Transactions of the Royal Society A264 (1151) (1969) 321–342.
[6] M.J. Lighthill, On sound generated aerodynamically, II: turbulence as a source of sound, Proceedings of the Royal Society A222 (1954) 1–32.
[7] K.S. Brentner, F. Farassat, An analytical comparison of the acoustic analogy and Kirchhoff formulation for moving surfaces, American Institute of Aeronautics and Astronautics Journal 36 (8) (1998) 1379–1386.
[8] D.P. Lockard, An efficient, two-dimensional implementation of the Ffowcs Williams and Hawkings equation, Journal of Sound and Vibration 229 (4) (2000) 897.